Available online at www.sciencedirect.com

SciVerse ScienceDirect

Ceramics International 39 (2013) 6057–6062

CERAMICS INTERNATIONAL

www.elsevier.com/locate/ceramint

Structural and electrical properties of $(Bi_{0.9}Dy_{0.1})(Fe_{0.975}TM_{0.025})O_{3\pm\delta}$ (TM = Ni^{2+}, Cr^{3+} and Ti^{4+}) thin films

C.M. Raghavan, E.S. Kim, J.W. Kim, S.S. Kim*

Department of Physics, Changwon National University, Changwon, Geongnam 641 773, Republic of Korea

Received 20 November 2012; received in revised form 9 January 2013; accepted 9 January 2013
Available online 17 January 2013

Abstract

Pure $BiFeO_3$ and rare earth and transition metal ions co-doped $(Bi_{0.9}Dy_{0.1})(Fe_{0.975}TM_{0.025})O_{3\pm\delta}$ (TM = Ni^{2+}, Cr^{3+} and Ti^{4+}) thin films were prepared on Pt(111)/Ti/SiO_2/Si(100) substrates by using a chemical solution deposition method. The changes in the microstructure and the electrical properties with doping elements were investigated. The thin films were well crystallized and randomly oriented, with no detectable impurity and secondary phases. The leakage current densities were reduced and the ferroelectric properties were improved in the co-doped thin films. Among the thin films, the $(Bi_{0.9}Dy_{0.1})(Fe_{0.975}Cr_{0.025})O_3$ thin film exhibited well saturated hysteresis loops with remnant polarization ($2P_r$) of 36 μC/cm^2 and coercive electric field ($2E_c$) of 954 kV/cm at 1000 kV/cm and low leakage current density of 1.91×10^{-5} A/cm^2 at 100 kV/cm. The enhanced properties observed in the co-doped thin films could be considered as being the result of the suppression of oxygen vacancies and of the modified microstructure.

Keywords: A. Films; C. Electrical properties; C. Ferroelectric properties; D. Perovskites

1. Introduction

It is well known that, among various multiferroic materials, perovskite bismuth ferrite $BiFeO_3$ (BFO) exhibits strong coupling between structural, ferroelectric and antiferromagnetic orders at room temperature [1,2]. Its remnant polarization (P_r) and out-of-plane converse piezoelectric coefficient d_{33} are comparable to those of the tetragonal, Ti-rich Pb(Zr,Ti)O_3 (PZT) system. Hence, BFO was already proposed as an alternative of toxic and currently utilizing ferroelectric PZT [3]. On comparing bulk BFO, in thin film form it exhibits large ferroelectric polarization owing to the small change in the lattice parameter [4]. In BFO, large electrical leakage, high coercive field, ferroelectric reliability and inhomogeneous magnetic spin structure are considered as major obstacles for the fabrication of practical devices [5]. Therefore, it is technologically important to improve electrical and ferroelectric properties of the perovskite BFO to completely overcome the toxic lead based PZT in ferroelectric devices. Presence of oxygen vacancies, formation of secondary phases, Fe^{2+}/Fe^{3+} valence fluctuation and poor microstructure are the crucial factors for the large electrical leakage in ferroelectric BFO [6–9]. There are flurry of ongoing researches to control the electrical leakage via different approaches [10]. Among all, cationic substitution into Bi- and Fe-sites of the BFO using rare earth (RE) and transition metal (TM) ions is strongly recommended for an effective reduction of leakage current density and increase of ferroelectric polarization [11–13]. The doping elements are also reported to alter the cycloid spin structure in turn enhances the magnetization of the BFO [11].

In this study, pure $BiFeO_3$ and co-doped $(Bi_{0.9}Dy_{0.1})(Fe_{0.975}TM_{0.025})O_{3\pm\delta}$ (TM = Ni^{2+}, Cr^{3+} and Ti^{4+}) thin films were prepared on Pt(111)/Ti/SiO_2/Si(100) substrates by using a chemical solution deposition method. The doping effects on the microstructural properties of the co-doped thin films were investigated by using X-ray diffraction patterns, Raman spectra and scanning electron microscopy. The electrical and the ferroelectric properties

*Corresponding author. Tel.: +82 552133421; fax: +82 552670264.
E-mail address: sskim@changwon.ac.kr (S.S. Kim).

0272-8842/$ - see front matter © 2013 Elsevier Ltd and Techna Group S.r.l. All rights reserved.
http://dx.doi.org/10.1016/j.ceramint.2013.01.022

for the co-doped thin films were also investigated and the results are discussed in detail.

2. Experimental procedure

The raw materials used for the precursor solutions were bismuth nitrate pentahydrate ($Bi(NO_3)_3 \cdot 5H_2O$) (99.99%), iron nitrate nonahydrate ($Fe(NO_3)_3 \cdot 9H_2O$) (99.99%), dysprosium nitrate hexahydrate ($Dy(NO_3)_3 \cdot 6H_2O$) (99.999%), nickel nitrate hexahydrate ($Ni(NO_3)_2 \cdot 6H_2O$) (99.99%), chromium nitrate nonahydrate ($Cr(NO_3)_3 \cdot 9H_2O$) and titanium isopropoxide [$Ti(OCH(CH_3)_2)_4$]. Ethylene glycol (99.99%) and 2-methoxyethanol (99.9%) were mixed together by constant stirring at 40 °C in a water bath for 30 min and used as a solvent. Bismuth nitrate pentahydrate (5 mol% excess) was added to the mixed solvent and stirred for 30 min. To the above Bi-solution acetic acid (99.99%) was added to catalyze the reaction and stirred for 30 min in turn. Finally, iron nitrate nonahydrate was added to form the BFO precursor solution. The resulting solution was subjected to continuous stirring for 3 h at room temperature. For the doping experiments, before the addition of iron nitrate nonahydrate, a measured quantity of dysprosium nitrate hexahydrate was added to the Bi-solution separately, transition metal nitrate was added to the Bi–Dy-solution and stirred for 30 min in turn. The resulting mixture was stirred for 3 h at room temperature. In the case of Ti doping, the reactions were conducted in glove box due to moisture sensitivity of titanium isopropoxide. The concentrations of all final solutions were adjusted to 0.1 M.

Pure and co-doped BFO thin films were deposited on $Pt(111)/Ti/SiO_2/Si(100)$ substrates (Inostek, Korea) by using a spin coating method at a constant spinning rate of 3000 rpm for 20 s. After spin coating, the wet thin films were prebaked at 360 °C for 10 min on a hot plate. The coating and the prebaking were repeated 12 times to obtain the desired film thickness. Finally, all thin films were subjected to conventional annealing at 550 °C for 30 min under a nitrogen atmosphere for crystallization.

Platinum (Pt) electrodes with areas of 1.54×10^{-4} cm^2 were deposited on the top surface of the thin films by ion sputtering through a metal shadow mask to form a capacitor structure. The structures of the thin films were investigated by using an X-ray diffractometer (Rigaku, MiniFlex II) and a Raman spectroscope (Jasco, NRS-3100). Surface morphologies and film thicknesses were analyzed by using a field emission scanning electron microscope (Tescan, MIRA II LMH). The ferroelectric hysteresis loops of the thin films were measured at a frequency of 10 kHz with triangular pulses by using a standardized ferroelectric test system (Modified Sawyer-Tower circuit with oscilloscope). The leakage current densities of the thin films were measured by using an electrometer (Keithley, 6517A). The dielectric properties of the thin films were studied by using an LF impedance phase analyzer (HP, 4192A).

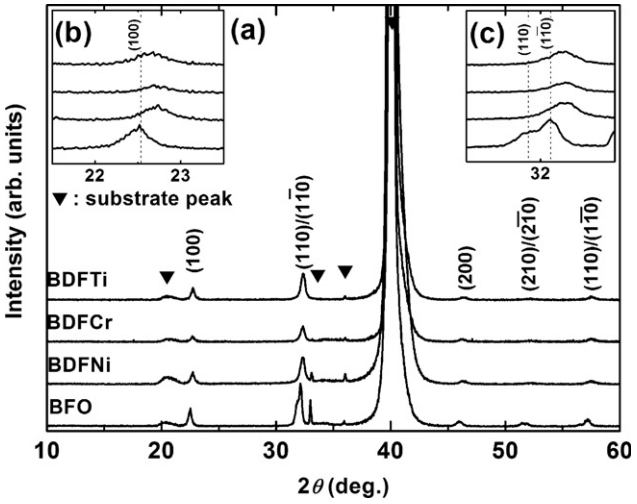

Fig. 1. XRD patterns of the BFO, BDFNi, BDFCr and BDFTi thin films deposited on $Pt(111)/Ti/SiO_2/Si(100)$ substrates. Magnified XRD patterns in the vicinities of (a) $2\theta = 22.5^\circ$ corresponding to (100) plane and (b) $2\theta = 32.0^\circ$ corresponding to (110)/(1$\bar{1}$0) planes to observe the lattice distortion in the BDFNi, BDFCr and BDFTi thin films.

3. Results and discussion

The X-ray diffraction (XRD) patterns of the pure $BiFeO_3$ (BFO) and the rare earth and transition metal co-doped $(Bi_{0.9}Dy_{0.1})(Fe_{0.975}TM_{0.025})O_{3 \pm \delta}$ (TM = Ni, Cr and Ti, denoted by BDFNi, BDFCr and BDFTi) thin films deposited on $Pt(111)/Ti/SiO_2/Si(100)$ substrates are shown in Fig. 1(a). The reflection peaks of the thin films were indexed with reference to the perovskite BFO structure [JCPDS no. 72-2035]. From the XRD analysis, for all thin films, randomly oriented polycrystalline distorted rhombohedral perovskite structure has been observed. There were no additional peaks corresponds to the secondary or impurity phases. This indicates that the dopant concentrations do not reach the solubility limit of BFO. From the magnified XRD patterns (Figs. 1(b) and (c)), the mild higher angle shifts in the peak position at the 2θ values of 22.5° (100) and 32° (100)/(1$\bar{1}$ QUOTE 0) were clearly observed for the co-doped thin films. This indicates changes in the lattice parameters of the co-doped thin films. In addition, the diffraction peaks corresponding to (100)/(1 QUOTE $\bar{1}$0) planes were clearly separated for the pure BFO thin film while the peaks were appeared as broad in the co-doped thin films (Fig. 1(c)). The change in lattice parameters and the peak broadening imply distortion in the rhombohedral lattice due to the incorporation of co-doping elements [11].

Fig. 2 shows the Raman scattering spectra for the pure BFO and the co-doped thin films measured at room temperature. According to the group theory, there are 13 ($4A_1 + 9E$) active modes predicted for the rhombohedrally distorted space group *R*3c [14]. All of the Raman modes observed in the pure BFO and the co-doped thin films are in good agreement with those for the rhombohedrally distorted (*R3c*) perovskite structure. By fitting the measured spectra and decomposing the fitted curves into individual Lorentz

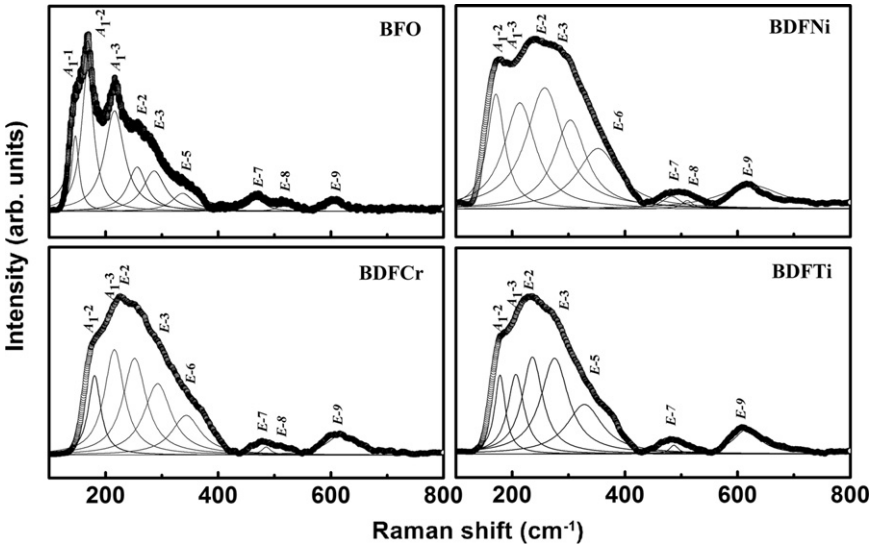

Fig. 2. Raman scattering spectra with decomposed active modes of the BFO, BDFNi, BDFCr and BDFTi thin films.

Table 1
Assignment and comparison of the observed Raman frequencies of the BFO, BDFNi, BDFCr and BDFTi thin films.

	Assigned Raman modes (cm^{-1})									
	A_1-1	A_1-2	A_1-3	*E*-2	*E*-3	*E*-5	*E*-6	*E*-7	*E*-8	*E*-8
BFO	147	168	216	256	287	337	–	469	517	607
BDFNi	–	170	214	258-	274	332	358	–	494	614
BDFCr	–	177	216	251-	275	335	359	–	495	618
BDFTi	–	178	209	243-	275	334	–	–	491	615

components, the peak positions have been obtained. The Raman modes observed in the low frequency region are attributed to the Bi–O vibration and the high frequency *E* modes are related to the Fe–O vibration [15]. As shown in Fig. 2, for the co-doped thin film, the changes in peak intensity and the peak broadening were observed at low frequencies. These are attributed to the dispersion of the Bi–O bonding by doping of rare earth Dy^{3+} ion for Bi sites [16]. The ionic radius of the Dy^{3+} (1.25 Å) is smaller than that of the Bi^{3+} (1.45 Å). Therefore, Dy can readily substitute into the Bi-site. The Dy substitution leads to the distortion in Bi–O bonding, which in turn broadened the low frequency A_1 modes of the co-doped BFO [17]. The small shifts in the peak positions at high frequencies for the co-doped thin films might be related to the transition metal dopants on the Fe-sites [18]. All the Raman active modes for the pure and the co-doped thin films are given in Table 1.

Fig. 3 shows the surface morphologies and the cross-sectional micrographs of the BFO BDFNi, BDFCr and BDFTi thin films. The difference in surface morphologies of the co-doped thin films compared to the pure BFO clearly implies that influence of rare earth and transition metal ions on the nucleation of BFO. From the top view of the SEM images, larger grains were observed in the pure BFO. In the case of the co-doped thin films, the grain size was found to be reduced and the smaller grains aggregate as grains-cluster. Decrease of grain size in the co-doped thin films can be explained by the decrease of oxygen vacancies, which results in lowering oxygen motion and consequently reduces grain growth rate [18–20]. In addition, both rare earth and transition metal ions may also act as heterogeneous nucleation centers for the perovskite structure, which in turn result grain size reduction and aggregation [19]. The thicknesses of the thin films measured from the SEM cross-sectional micrographs were approximately 300 nm (BFO) and 400 nm (BDFNi, BDFCr and BDFTi), respectively.

The leakage current densities (*J*) versus applied electric fields (*E*) for the pure and the co-doped thin films measured at room temperature are shown in Fig. 4(a). The co-doped thin films exhibited low leakage current densities compared to the pure BFO thin film over the entire applied electric field region. The measured leakage current densities of the BFO, BDFNi, BDFCr and BDFTi thin films at 100 kV/cm were 2.58×10^{-3}, 8.62×10^{-5}, 1.91×10^{-5} A/cm^2 and 5.71×10^{-5} A/cm^2, respectively. The measured leakage current densities of the co-doped thin films were two orders lower than that of the pure BFO thin film. The decrease of leakage current densities in the co-doped thin films is attributed to the decrease of the oxygen vacancies by doping of rare earth and transition metal ions [21]. The BFO thin film is reported to exhibit

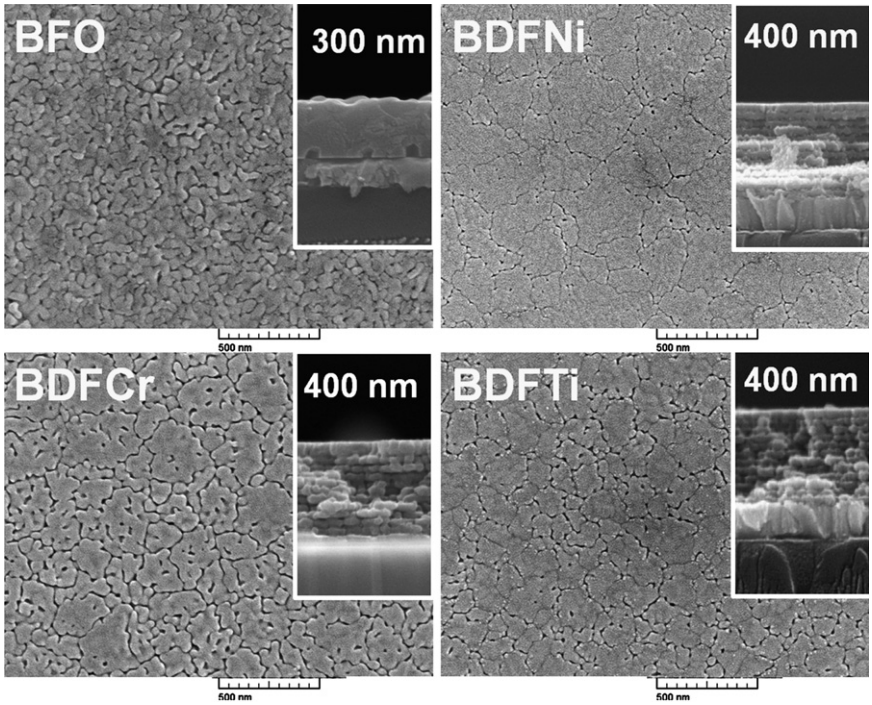

Fig. 3. SEM morphologies of the BFO, BDFNi, BDFCr and BDFTi thin films containing cross-sectional micrographs.

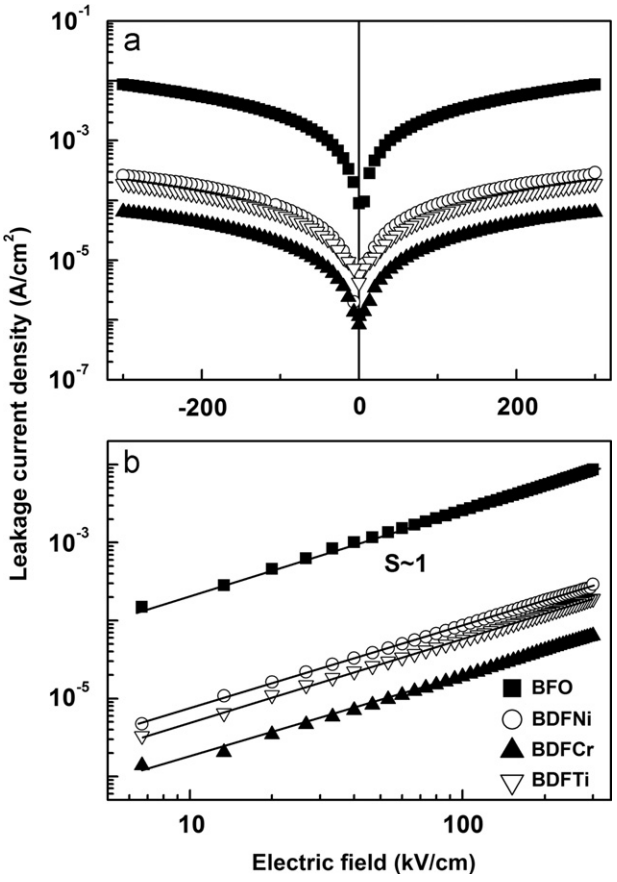

Fig. 4. (a) Leakage current densities of the BFO, BDFNi, BDFCr and BDFTi thin films and (b) log(J)–log(E) characteristics of the thin films.

high leakage current due to poor microstructure, small amount of Fe^{2+} species, charge defects (oxygen and Bi vacancies) and nonstoichiometry. The formations of oxygen and Bi vacancies and Fe charge fluctuation (Fe^{2+}/Fe^{3+}) are given in the following Kröger–Vink notations [22,23].

$$2Bi_{Bi}^{\times} + 3O_O^{\times} \rightarrow 2V_{Bi}^{'''} + 3V_O^{\bullet\bullet} + Bi_2O_3$$

$$O_O^{\times} + 2Fe_{Fe}^{\times} \rightarrow (1/2)O_2 + 2Fe_{Fe}^{'} + V_O^{\bullet\bullet}$$

where $Bi_{Bi}^{\times}$, $Fe_{Fe}^{\times}$ and $O_O^{\times}$ are the Bi, Fe and oxygen ions in lattice, $V_{Bi}^{'''}$ and $V_O^{\bullet\bullet}$ indicate Bi and oxygen vacancies with three negative and two positive charges, $Fe_{Fe}^{'}$ represents Fe^{2+} ion with one negative charge. The Bi and oxygen vacancies act as current pass in BFO. The formation of Fe^{2+} leads electrons hopping between Fe^{2+} and Fe^{3+} through oxygen vacancies. The oxygen vacancies act as a "bridge" between Fe^{2+} and Fe^{3+}, which in turn increase electrical leakage in BFO [24]. Therefore, the reduced leakage current densities in the co-doped thin films may be related to the reduced oxygen vacancies. The bond dissociation energy of the Dy–O (611 ± 42 kJ/mol) is higher than that of the Bi–O (343 ± 6 kJ/mol), hence, doping of the rare earth Dy^{3+} ion into Bi-site of the BFO can control the Bi evaporation and stabilize the perovskite structure [21]. Among the thin films, the BDFCr thin film showed the lowest leakage current density. The low J value for the BDFCr thin film might be attributed substitution of stable Cr^{3+} for the electronically unstable Fe^{3+} ion. In addition, the [FeO_6] octahedra are isostructural with [CrO_6] octahedra [25]. Hence, co-doping of Cr into Fe-site controls the charge fluctuation and reduces the

electrical leakage. The divalent Ni^{2+} favors formation of oxygen vacancies and leads more leakage compared to the BDFCr and BDFTi thin films [13]. However, divalent Ni^{2+} ion co-doping into the perovskite BFO avoids the formation of Fe^{2+} ion and decreases the J value compared to the pure BFO. The higher valence Ti^{4+} in Fe-sites involves filling the oxygen vacancies by replacing electrically unstable Fe^{3+} ions [13]. Therefore, the decrease in the leakage current density in the co-doped thin films is attributed to a reduction in the number of oxygen vacancies. The leakage current mechanism was analyzed by using logarithmic plots of current density versus applied electric field ($\log(J)-\log(E)$) as shown in Fig. 4(b). The linearity of the lines over the entire region of applied electric field for the pure and the co-doped thin films with the slope value $\sim$1.0 indicates Ohmic conduction mechanism and is dominated by thermally stimulated free electrons [2]. The leakage current for Ohmic conduction can be expressed as

$$J = e\mu N_e E,$$

where e is the electron charge, μ is the free carrier mobility, N_e is the density of the thermally stimulated electrons and E is the applied electric field.

The ferroelectric polarization–electric field (P–E) hysteresis loops of the BFO, BDFNi, BDFCr and BDFTi thin films are shown in Fig. 5. The co-doped thin films showed improved ferroelectric properties compared to the pure BFO thin film. The low remnant polarization ($2P_r$) of 28 μC/cm^2 and the large coercive field ($2E_c$) of 1376 kV/cm at an applied electric field of 1066 kV/cm were observed for the pure BFO thin film. The $2P_r$ and the $2E_c$ values of the BDFNi, BDFCr and BDFTi thin films were 38 μC/cm^2 and 937 kV/cm, 36 μC/cm^2 and 954 kV/cm and 49 μC/cm^2 and 1070 kV/cm at an applied electric field of 1000 kV/cm, respectively. The increase of $2P_r$ and the decrease of $2E_c$ for the co-doped thin films are well correlated with the low leakage current density compared to the pure BFO thin film. In addition to this, the lattice distortions due to the Dy doping into Bi-site enhance the ferroelectric polarization [11]. On comparing Dy alone doped BFO, the (Dy, TM) co-doped BFO thin films exhibit significantly improved ferroelectric properties [26]. This indicates the crucial role of the transition metal ions for the further improvement of the electrical and the ferroelectric properties. Among the co-doped thin films, the BDFCr thin film showed well shaped hysteresis loops with low coercive field and increased polarization.

The frequency dependent dielectric properties of the thin films measured at room temperature in the frequency range of 100 Hz to 1 MHz are shown in Fig. 6. The dielectric constants of all thin films gradually decreased with increasing frequency. The dielectric constant and the dielectric loss values for the BFO, BDFNi, BDFCr and BDFTi thin films were 121 and 0.049, 130 and 0.042, 145 and 0.039 and 124 and 0.043 at 1 kHz, respectively. Large dielectric constants and low dielectric losses for the co-doped thin films are correlated with the low leakage current density.

Compared to the divalent Ni^{2+} and tetravalent Ti^{4+} ions, the co-doping of trivalent Cr^{3+} for electronically unstable Fe^{3+} can stabilize the perovskite structure by suppressing the charge fluctuation (Fe^{2+}/Fe^{3+}) in the BFO. In overall consideration, the reduction of leakage current density, shape perfection in the hysteresis loops and improved dielectric properties of the BDFCr implies, the specific role of Cr doping in the improvement of electrical and ferroelectric properties of the BFO.

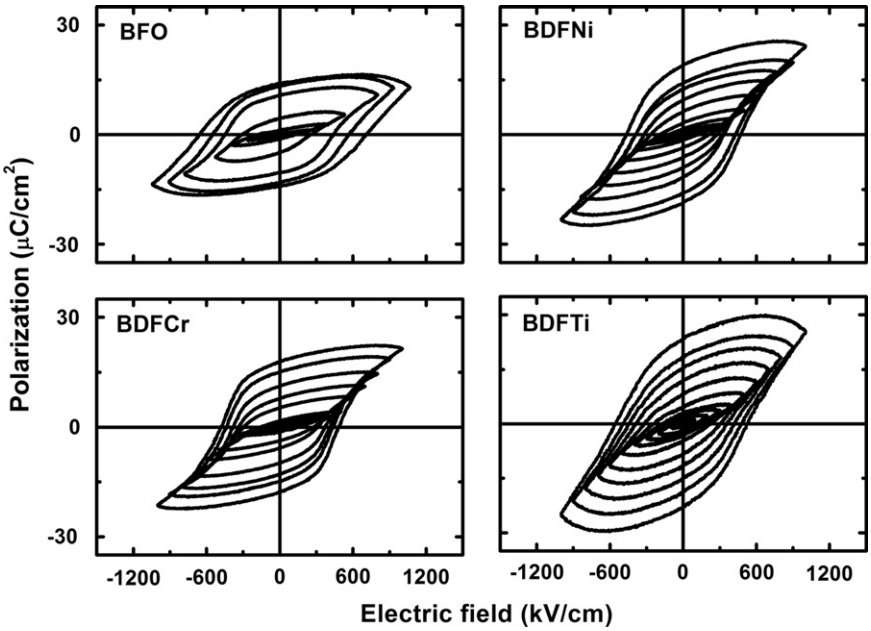

Fig. 5. Ferroelectric P–E hysteresis loops of the BFO, BDFNi, BDFCr and BDFTi thin films.

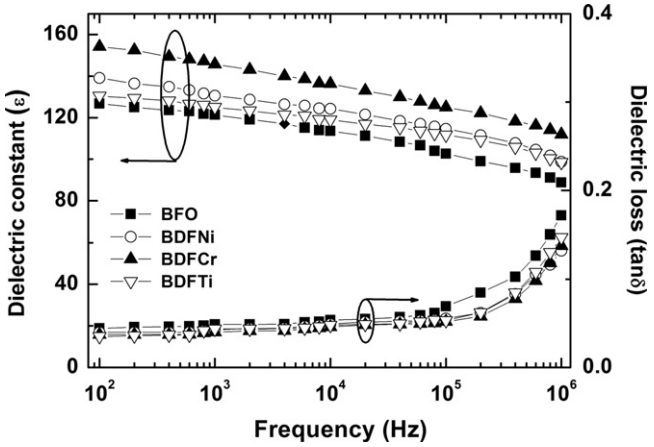

Fig. 6. Dielectric behaviors of the BFO, BDFNi, BDFCr and BDFTi thin films.

4. Conclusions

Effects of (Dy, TM) (TM = Ni, Cr and Ti) co-doping on the structural, electrical and ferroelectric properties of the BFO thin films prepared on Pt(111)/Ti/SiO_2/Si(100) substrates via a chemical solution deposition were investigated. The distorted rhombohedral perovskite structures for the pure BFO and the co-doped thin films were confirmed by using an XRD and a Raman scattering analysis. Significant improvements, such as reduced leakage current density and coercive field, were observed for the co-doped thin films. The leakage current density was reduced and the ferroelectric properties were improved in the co-doped thin films. The enhanced properties could be explained by the combined effects of reduced oxygen vacancies and modified microstructure.

Acknowledgments

This work was supported by Priority Research Centers Program through the National Research Foundation of Korea (NRF) funded by the Ministry of Education, Science and Technology (2010–0029634).

References

[1] T. Zhao, A. Scholl, F. ZavaLiche, K. Lee, M. Barry, A. Doran, M.P. Cruz, Y.H. Chu, C. Ederer, N.A. Spaldin, R.R. Das, D.M. Kim, S.H. Baek, C.B. Eom, R. Ramesh, Electrical control of antiferromagnetic domains in multiferroic $BiFeO_3$ films at room temperature, Nature Materials 5 (2006) 823.

[2] G.W. Pabst, L.W. Martin, Y.H. Chu, R. Ramesh, Leakage mechanisms in $BiFeO_3$ thin films, Applied Physics Letters 90 (2007) 072902.

[3] Y.H. Chu, Q. Zhan, L.W. Martin, M.P. Cruz, P.L. Yang, G.W. Pabst, F. Zavaliche, S.Y. Yang, J.X. Zhang, L.Q. Chen, D.G. Schlom, I.N. Lin, T.B. Wu, R. Ramesh, Nanoscale domain control in multiferroic $BiFeO_3$ thin films, Advanced Materials 18 (2006) 2307.

[4] J.B. Neaton, C. Ederer, U.V. Waghmare, N.A. Spaldin, K.M. Rabe, First-principles study of spontaneous polarization in multiferroic $BiFeO_3$, Physical Review B 71 (2005) 014113.

[5] D. Hong, S. Yu, J. Cheng, Sm–Ti co-substituted $BiFeO_3$ thin films prepared by sol–gel technique, Current Applied Physics 11 (2011) S255.

[6] S.K. Singh, H. Ishiwara, K. Maruyama, Enhanced polarization and reduced leakage current in $BiFeO_3$ thin films fabricated by chemical solution deposition, Applied Physics Letters 100 (2006) 064102.

[7] H. Ishiwara, Impurity substitution effects in $BiFeO_3$ thin films-From a viewpoint of FeRAM applications, Current Applied Physics 12 (2012) 603.

[8] C.M. Raghavan, D. Do, J.W. Kim, W.-J. Kim, S.S. Kim, Effects of transition metal ion doping on structure and electrical properties of $Bi_{0.9}Eu_{0.1}FeO_3$ thin films, Journal of American Ceramic Society 95 (2012) 1933.

[9] J. Liu, M. Li, L. Pei, B. Yu, D. Guo, X. Zhao, Effect of Ce doping on the microstructure and electrical properties of $BiFeO_3$ thin films prepared by chemical solution deposition, Journal of Physics D: Applied Physics 42 (2009) 115409.

[10] J. Wu, G. Kang, J. Wang, Electrical behavior and oxygen vacancies in $BiFeO_3/[(Bi_{1/2}Na_{1/2})_{0.94}Ba_{0.06}]TiO_3$ thin film, Applied Physics Letters 95 (2009) 192901.

[11] F. Yan, M.O. Lai, L. Lu, T.J. Zhu, Enhanced multiferroic properties and valence effect of Ru-doped $BiFeO_3$ thin films, Journal of Physical Chemistry C 114 (2010) 6994.

[12] P. Kharel, S. Talebi, B. Ramachandran, A. Dixit, V.M. Naik, M.B. Sahana, C. Sudakar, R. Naik, M.S.R Rao, G. Lawes, Structural, magnetic, and electrical studies on polycrystalline transition-metal-doped $BiFeO_3$ thin films, Journal of Physics: Condensed Matter 21 (2009) 036001.

[13] X. Qi, J. Dho, R. Tomov, M.G. Blamire, J.L.M. Driscoll, Greatly reduced leakage current and conduction mechanism in aliovalent-ion-doped $BiFeO_3$, Applied Physics Letters 86 (2005) 062903.

[14] M.K. Singh, H.M. Jang, S. Ryu, M.H. Jo, Polarized Raman scattering of multiferroic $BiFeO_3$ epitaxial films with rhombohedral *R3c* symmetry, Applied Physics Letters 88 (2006) 042907.

[15] P. Hermet, M. Goffinet, J. Kreisel, Ph. Ghosez, Raman and infrared spectra of multiferroic bismuth ferrite from first principles, Physical Review B 75 (2007) 220102.

[16] N. Jeon, D. Rout, I.W. Kim, S.J.L. Kang, Enhanced multiferroic properties of single-phase $BiFeO_3$ bulk ceramics by Ho doping, Applied Physics Letters 98 (2011) 072901.

[17] G. Kartopu, A. Lahmar, S. Habouti, C.L. Solterbeck, B. Elouadi, M. Es-Souni, Observation of structural transitions and Jahn–Teller distortion in $LaMnO_3$-doped $BiFeO_3$ thin films, Applied Physics Letters 92 (2008) 151910.

[18] A.Z. Simões, R.F. Pianno, E.C. Aguiar, E. Longo, J.A Varela, Effect of niobium dopant on fatigue characteristics of $BiFeO_3$ thin films grown on Pt electrodes, Journal of Alloys and Compounds 479 (2009) 274.

[19] C.F. Chung, J.P. Lin, J.M. Wu, Influence of Mn and Nb dopants on electric properties of chemical-solution-deposited $BiFeO_3$ films, Applied Physics Letters 88 (2006) 242909.

[20] G.L. Song, H.X. Zhang, T.X. Wang, H.G Yang, F.G. Chang, Effect of Sm, Co codoping on the dielectric and magnetoelectric properties of $BiFeO_3$ polycrystalline ceramics, Journal of Magnetism and Magnetic Materials 324 (2012) 2121.

[21] Q. Ke, X. Lou, Y. Wang, J. Wang, Oxygen-vacancy-related relaxation and scaling behaviors of $Bi_{0.9}La_{0.1}Fe_{0.98}Mg_{0.02}O_3$ ferroelectric thin films, Physical Review B 82 (2010) 024102.

[22] S.R. Basu, L.W. Martin, Y.H. Chu, M. Gajek, R. Ramesh, R.C. Rai, X. Xu, J.L. Musfeldt, Photoconductivity in $BiFeO_3$ thin films, Applied Physics Letters 92 (2008) 091905.

[23] A. Lahmar, K. Zhao, S. Habouti, M. Dietze, C.-H. Solterbeck, M. Es-Souni, Off-stoichiometry effects on $BiFeO_3$ thin films, Solid State Ionics 202 (2011) 1.

[24] G.L. Yuan, S.W. Or, Enhanced piezoelectric and pyroelectric effects in single-phase multiferroic $Bi_{1-x}Nd_xFeO_3$ (x=0–0.15) ceramics, Applied Physics Letters 88 (2006) 062905.

[25] T. Nozaki, K. Hayashi, T. Kajitani, Mn-substitution effect on thermal conductivity of Delafossite-type oxide $CuFeO_2$, Journal of Electronic Materials 39 (2010) 1798.

[26] P. Uniyal, K.L. Yadav, Observation of the room temperature magnetoelectric effect in Dy doped $BiFeO_3$, Journal of Physics: Condensed Matter 21 (2009) 012205.